Stability Analysis for the Head-Disk Interface in a Flexible Disk Drive

Kyosuke Ono[1]

Jen-San Chen

D. B. Bogy
Mem. ASME

Computer Mechanics Laboratory,
Department of Mechanical Engineering,
University of California,
Berkeley, CA 94720

This paper describes the modeling, theoretical formulation, and eigenvalue analysis for a combined system of a spinning flexible disk and a pair of head and suspension systems that contact the disk at opposing points on its two sides. In the analytical model a constant friction force between the sliders and disk and the slider pitch motion, as well as its transverse motion, are taken into account. From the eigenvalue analysis it is found that pitch stiffness and moment of inertia of the heads induce instability above the critical rotation speed similarly to the transverse stiffness and mass. This instability can be effectively stabilized by increasing the external damping which is spinning with the disk. It is also found that the friction force makes all forward modes unstable over the entire rotational speed range. The friction induced instability can be effectively suppressed by increasing the transverse stiffness and mass and it can be stabilized by the pitch damping and the external damping. The characteristics of instability due to the friction force qualitatively agree well with experimental results reported previously.

Introduction

Flexible disk storage systems have been widely used as convenient input/output devices in data processing systems, especially in small personal computers. To meet user demand for convenient removable media, smaller size and larger capacity flexible disk drives have been developed in the past 20 years. Recent progress in the performance-to-cost ratio in computers and hard disk drives increases the need for development of a high speed and large capacity flexible disk storage system with more than ten megabytes.

The most difficult problem encountered in developing a new flexible disk drive is to obtain a stable and reliable scanning condition between the medium and recording head. The disk and head suspension often exhibit vibrations which cause not only malfunctions in the read/write signal but also a remarkable reduction of recording medium life. Until now this vibration has been suppressed through trial and error by changing the tribological characteristics of the medium, the slider contour and its suspension system. Therefore, efforts to understand the mechanism of vibration related to the head and flexible disk interface through analysis and to find a stable scanning condition has recently become of great concern for many researchers.

Vibrations of a spinning flexible disk induced by a point contact stationary head was investigated by Benson and Bogy (1978), Ono et al. (1986), and Ono and Maeno (1987). Benson and Bogy (1978) discussed different stationary deflection patterns of a spinning flexible disk depending on its thickness and the position of the head. Ono et al. (1986) analyzed stationary disk deflections associated with critical speeds for 8, 5.25, and 3.5-in. flexible disks, but they found qualitative discrepancies between theory and experiment. Ono and Maeno (1987) found that the steady deflection and vibrations of a 3.5-in. flexible disk induced by a point contact head can be qualitatively predicted by taking into account a residual compressible stress in the circumferential direction and an initial deflection of the disk.

As for the vibration of a coupled system of a spinning flexible disk with a head and suspension, Iwan and Moeller (1976) analyzed the instability of a spinning disk due to coupling effects of a translational mass, spring, and damper. They found three different instability regions above the critical speed due to the attached mass, spring, and damper, respectively. For the investigation of unstable head vibrations, Good and Lowery (1985) used finite element modeling and free vibration analysis of an actual disk and head assembly system. They included head pitch and roll motion as well as transverse motion and could get good agreement with experiment for the dominant mode frequencies, but they did not analyze the instability. A comprehensive experimental study of unstable vibration of an actual 5.25-in. flexible disk and head was reported by Kohno et al. (1989). Since the unstable vibration observed by them is related to the head pitch motion and appears to

[1]On sabbatical leave from the Tokyo Institute of Technology, Department of Mechanical Engineering, Meguro-ku, Tokyo, Japan.

Contributed by the Applied Mechanics Division of THE AMERICAN SOCIETY OF MECHANICAL ENGINEERS for presentation at the Joint Applied Mechanics/Bioengineering Conference, Ohio State University, Columbus, Ohio, June 16-19, 1991.

Discussion of this paper should be addressed to the Technical Editor, Prof. Leon M. Keer, The Technological Institute, Northwestern University, Evanston, IL 60208, and will be accepted until two months after final publication of the paper itself in the JOURNAL OF APPLIED MECHANICS. Manuscript received by the ASME Applied Mechanics Division, June 4, 1990; final revision, Aug. 16, 1990.

Paper No. 91-APM-31.

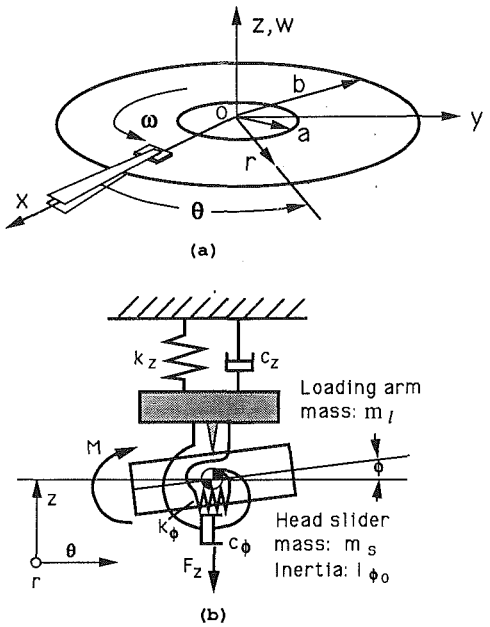

Fig. 1 Model of flexible disk and head assembly system; (*a*) Spinning flexible disk, head assemblies, and fixed coordinate system; (*b*) Model of upper and lower head assemblies

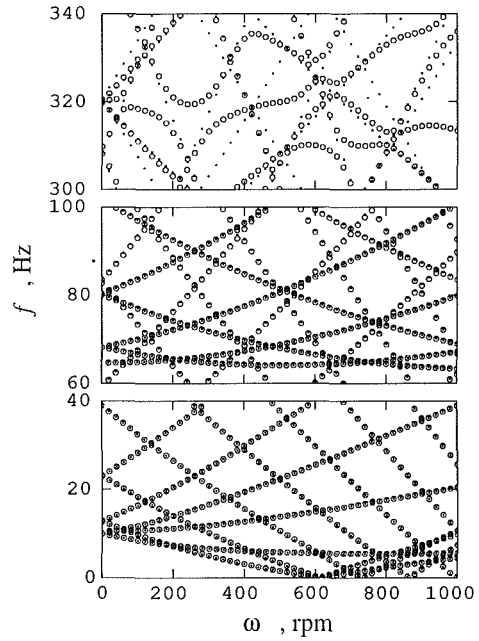

Fig. 2 The pitch moment of inertia and small pitch stiffness effects on the natural frequency ($I_\phi = I_{\phi 0}$, $k_\phi = 10 \times k_{\phi 0}$ [f_ϕ = 31.6 Hz])

occur far below the lowest critical speed, it appears to be unrelated to the instability phenomena predicted by Iwan and Moeller (1976). Jiang and Chonan (1989) theoretically obtained many unstable regions below the lowest critical speed for a coupled system of a flexible disk and a translational mass and spring. However, the unstable vibrations observed by Kohno et al. cannot be explained by the results obtained by Jiang and Chonan, because the relationship between unstable frequency and rotational speed is qualitatively different in the two studies. In addition, the pitch motion of the head was not considered in their analysis. Moreover, the unstable regions below the critical speed in Jiang and Chonan appear to result from mistreatment in their theoretical formulation of a stationary force applied to the spinning disk by the head.

In view of the discrepancy between theory and experiment for the unstable vibration related to head-to-medium interface as stated above, an effort is made here to develop a more accurate model of a flexible disk and head assembly system which has the potential to eliminate this discrepancy. This paper presents the theoretical formulation and eigenvalue analysis for an extended model where the pitch motion of the head and friction force between the heads and medium are taken into account. Although an actual head-to-medium interface and suspension system are more complex than the present model, it is hoped that this work will contribute to a better physical insight into unstable vibrations in the head-to-medium interface in flexible disk systems.

Analytical Model and Theoretical Formulation

Figure 1 portrays an analytical model of a coupled system of a spinning flexible disk and upper and lower head assemblies, together with the fixed coordinate systems *O-xyz*, *O-rθz* and physical parameters considered in this model. In order to simplify the analytical model while not losing important factors relevant to the instability phenomena, the following assumptions are made with respect to the head-to-medium interface and head assemblies.

1 Identical upper and lower heads are sliding on the disk with equal and opposite static loads F_{z0} and with no initial static disk deflection.

2 The upper and lower head sliders move together as a rigid body in the transverse and pitch directions in contact with the disk. The lower head slider is stiffly supported in the transverse direction, whereas the upper one is loaded on the disk by a flexible spring through a suspension arm. Thus, the effective transverse mass m_z is the sum of the two slider masses m_s and the mass of the loading arm m_l in a normal operating condition. The pitch moment of inertia I_ϕ is related to the two head sliders whose mass center G is in the middle plane of the disk. The head sliders are not allowed to move in the direction parallel to the disk surface. The roll motion of the head slider about an axis in the circumferential direction is not coupled to other motions and can be omitted for the stability analysis.

3 The suspension system of the two head assemblies is modeled as a simple transverse spring with stiffness coefficient k_z and damper with damping coefficient c_z together with a pitch moment spring k_ϕ and damper c_ϕ. They are uncoupled from each other.

4 The acting and reacting forces and moment between the disk and a pair of head sliders are transverse force F_z, friction force F_θ and pitch moment M. They are concentrated at the mass center G of the two head sliders.

5 The friction force F_θ is constant and given by $2\mu F_{z0}$, where μ is the friction coefficient.

Even when the disk is rotating in air without any constraint such as a liner, the surrounding air has some inertia and damping effects on the disk vibration, especially in the high-frequency region. Estimation of these effects is not easy and is itself a subject to be studied. The mass effect of the surrounding air may be equivalently understood not only as an additional spinning mass of the disk, but also as a stationary mass which is attached to the disk like the two heads. However, because of the difficulty of its qualitative estimation, the mass effect of the surrounding air is neglected here. Although the estimation of the damping effect of the surrounding air is also difficult, we simply regard it as two kinds of homogeneous external damping; one of them is spinning with the disk (c_1) and another is stationary (c_2).

From the infinitesimal analysis, the equation of motion of the disk can be written in terms of transverse displacement w and with respect to the stationary coordinate system (r, θ), as

$$\rho H\left(\frac{\partial}{\partial t}+\omega\frac{\partial}{\partial \theta}\right)^2 w + c_1\left(\frac{\partial}{\partial t}+\omega\frac{\partial}{\partial \theta}\right)w + c_2\frac{\partial w}{\partial t}$$

$$+D\nabla^4 w - H\frac{\partial}{r\partial r}\left(\sigma_r r\frac{\partial w}{\partial r}\right) - H\frac{\sigma_\theta}{r^2}\frac{\partial^2 w}{\partial\theta^2}$$

$$=\frac{1}{r}\left(F_z + F_\theta\frac{\partial w}{r\partial\theta}\right)\delta(r-\xi)\delta(\theta) - \frac{1}{r^2}\frac{\partial}{\partial\theta}[M\delta(\theta)]\delta(r-\xi) \quad (1)$$

where

$$D=\frac{EH^3}{12(1-\nu^2)}, \quad \nabla^2=\left(\frac{\partial^2}{\partial r^2}+\frac{1}{r}\frac{\partial}{\partial r}+\frac{1}{r^2}\frac{\partial^2}{\partial\theta^2}\right).$$

The parameters ρ, H, E, and ν are the density, thickness, Young's modulus, and Poisson's ratio of the disk. $\delta(:)$ is the Dirac delta function. The coupling position between heads and disk is assumed to be $r = \xi$ and $\theta = 0$. When the spinning disk is clamped at the inner radius $r = a$ and free at the outer radius $r = b$, the in-plane stresses σ_r and σ_θ due to the centrifugal effect are given by

$$\left.\begin{aligned}
&\sigma_r = C_1 + \frac{C_2}{r^2} + C_3 r^2, \ \sigma_\theta = C_1 - \frac{C_2}{r^2} + C_4 r^2\\
&C_1 = \frac{1+\nu}{8}\rho\omega^2\frac{(\nu-1)a^4-(3+\nu)b^4}{(\nu-1)a^2-(1+\nu)b^2}\\
&C_2 = \frac{1-\nu}{8}\rho\omega^2 a^2 b^2\frac{(1+\nu)a^2-(3+\nu)b^2}{(\nu-1)a^2-(1+\nu)b^2}\\
&C_3 = -\frac{3+\nu}{8}\rho\omega^2, \ C_4 = -\frac{1+3\nu}{8}\rho\omega^2
\end{aligned}\right\} \quad (2)$$

From Fig. 1(*b*), the dynamic transverse force F_z and pitching moment M are, respectively, given by

$$F_z = -m_z\frac{\partial^2 w}{\partial t^2} - c_z\frac{\partial w}{\partial t} - k_z w \quad (3)$$

$$M = -I_\phi\frac{\partial^2}{\partial t^2}\left(\frac{\partial w}{r\partial\theta}\right) - c_\phi\frac{\partial}{\partial t}\left(\frac{\partial w}{r\partial\theta}\right) - k_\phi\frac{\partial w}{r\partial\theta}. \quad (4)$$

Equation (1) looks like an inhomogeneous equation but becomes a homogeneous equation after substitution of equations (3) and (4) into equation (1).

A particular solution of the disk deflection for this homogeneous system is assumed in the form of a Fourier sine and cosine series expansion as follows:

$$w=\sum_{l=0}^{L}(G_l(r,t)\cos l\theta + K_l(r,t)\sin l\theta). \quad (5)$$

In the case of a freely spinning disk, the sine and cosine functions represent circumferential eigenmodes. In the case of the coupled system of the disk and head assembly, each eigenmode deviates from a harmonic function, but can be approximately expressed as a linear combination of harmonic functions. Regarding the mode functions' dependence on r, G_l, and K_l are obtained by the finite element method as described in a previous paper (Ono et al., 1986). This implies that the radial mode functions, which are decomposed into harmonic functions, are assumed to be approximately represented in the third-order polynomial function space within the region of each element.

Substituting the disk deflection (5) into the basic equations (1), (2), (3), and (4), we can get a set of partial differential equations for $G_l(r,t)$ and $K_l(r,t)$. Based on the finite element method, we next transform these differential equations with respect to r into matrix algebraic equations for the state vector at the nodes of the finite number of elements. When the element number in the r direction is denoted by N and the harmonic functions are taken into account up to $l = L$, the degrees-of-freedom of the final matrix equation for this coupled system becomes $2(1 + 2L)N$. Since the coefficient matrices of this second-order time-derivative equation are asymmetrical, the eigenvalue analysis was carried out by using an available library program of generalized eigenvalue analysis.

For the purpose of comparison with the theoretical and experimental works published previously, a 5.25-in. flexible disk is chosen for computer calculation, although the calculated data of the most prevailing 3.5-in. disk will be more interesting than for the 5.25-in. disk from a technical point of view. For the physical parameters of the disk, the following values are used in the calculation: $E = 4.9\times10^9$ N/m^2, $\nu = 0.3$, $\rho = 1.3\times10^3$ kg/m^3, $H = 0.078$ mm, $a = 17.5$ mm, $b = 65.0$ mm, and $\xi/b = 0.75$.

As for the head and suspension parameters, the mass m_s and pitching moment of inertia I_ϕ of the two sliders are estimated as 4.0×10^{-4} kg and 1.60×10^{-9} kg m^2, respectively. The effective transverse mass m_z including both slider mass m_s and the loading arm mass m_l are estimated as 4.0×10^{-3} kg; ten times larger than m_s. Then, 4.0×10^{-3} kg and 1.60×10^{-9} kg m^2 are, respectively, considered to be representative transverse mass and pitch moment of inertia, which we denote henceforth by m_{z0} and $I_{\phi0}$. Since the transverse mass m_z and pitch moment of inertia I_ϕ are not easily changed, their nominal values, m_{z0} and $I_{\phi0}$, are usually used in the following calculations.

On the other hand, the stiffness and damping of the suspension cannot be definitely estimated, since different manufacturers may choose quite different values. Especially, the stiffness can be changed so easily that its value may be selected from the view point of stability. Therefore, the effects of stiffness on the eigenvalues were investigated by using several different values in the calculation. In order to get better physical insight into the frequency characteristics of the coupled system, we first note the natural frequencies of the different subsystems. The lowest values of the transverse stiffness k_{z0} and pitch stiffness $k_{\phi0}$ are chosen to be 15.8 N/m and 6.32×10^{-6} Nm/rad, respectively, so that the transverse natural frequency f_z ($\equiv\sqrt{k_{z0}/m_z}/2\pi$) and the pitch natural frequency f_ϕ ($\equiv\sqrt{k_{\phi0}/I_\phi}/2\pi$) of the two head assemblies both become 10 Hz, when m_z is equal to m_{z0} ($= 4.0\times10^{-3}$ kg) and I_ϕ is equal to $I_{\phi0}$ ($= 1.60\times10^{-9}$ kg m^2), respectively.

The effect of the suspension damping is one of the most important concerns in this study, because it is well known that the singing noise has been often stabilized by the addition of some damping material to the suspension. Since it is not easy to increase the damping factor by a large amount, the effects of transverse and pitch damping are examined with the nondimensional damping ratio having the value 0.1. The effects of the external damping c_1 and c_2 are also investigated by choosing their values properly.

From the viewpoints of both computing efficiency and accuracy, the maximum number L of the order of the harmonic functions and the finite element number N is chosen to be 15 and 5, respectively. Eigenvalues are generally expressed in the form $\alpha \pm 2\pi fj$, where $j = \sqrt{-1}$. The real part α and the frequency f are plotted and discussed. The notation (n,l) represents the nth nodal circle and lth nodal diameter mode. Its forward and backward travelling components are expressed by the subscripts f and b, respectively.

Calculated Results and Discussion

(1) Pitch Moment of Inertia and Stiffness Effects. The coupling effects of a spinning disk and a pitch vibration system have not been investigated previously, and the effects of the pitch parameters in the real head assemblies are weak compared with those of the transverse parameters. Therefore, a coupled system, which includes only pitch moment of inertia and stiffness, is discussed first. Figure 2 shows the natural frequencies f of the coupled system (open circles) where the pitch moment of inertia I_ϕ is equal to $I_{\phi0}$ and the pitch stiffness k_ϕ is equal to $10\times k_{\phi0}$. Since the pitch frequency of the head and suspension system f_ϕ is 31.6 Hz in this case, the amount of k_ϕ is regarded as fairly small compared with actual cases. For com-

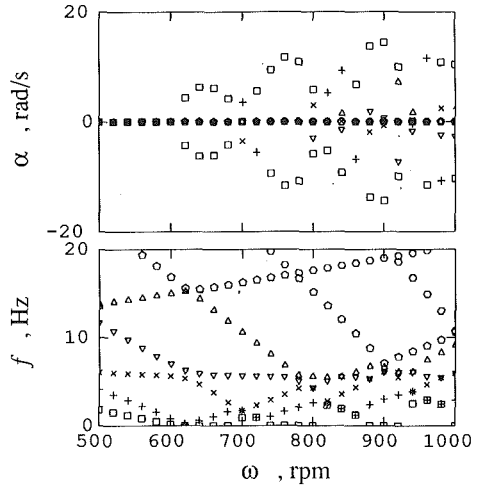

Fig. 3 Instability due to large pitch stiffness ($I_\phi = I_{\phi 0}$, $k_\phi = 10^3 \times k_{\phi 0}$ [f_ϕ = 316 Hz])

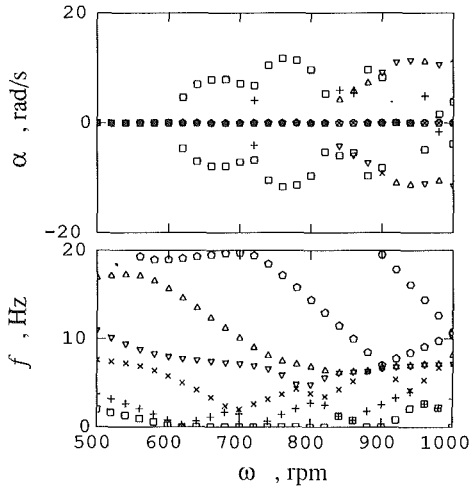

Fig. 5 Instability due to transverse mass and large transverse stiffness ($m_z = m_{z0}$, $k_z = 10^4 \times k_{z0}$ [f_z = 1.0 kHz])

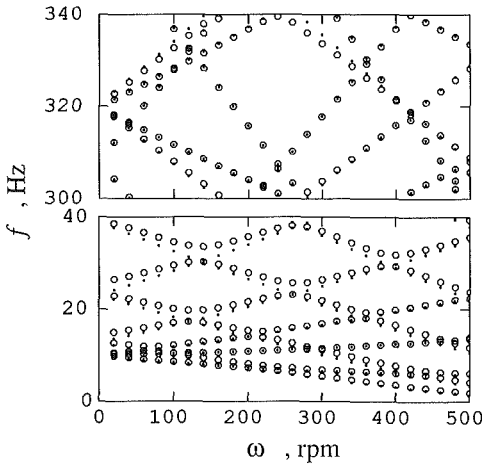

Fig. 4 The pitch moment of inertia and large pitch stiffness effects on the natural frequency ($I_\phi = I_{\phi 0}$, $k_\phi = 10^3 \times k_{\phi 0}$ [f_ϕ = 316 Hz])

parison the natural frequency of a free disk is indicated in Fig. 2 with small black dots. Since the real part of the eigenvalue is almost zero in this case, the α value is not shown here.

It is seen from this figure that a nonrotating 5.25-in. flexible disk has the lowest natural frequencies for the zero nodal circle modes (0,0) and (0,1) at about 10 Hz, while the lowest one nodal circle mode, i.e., the (1,0) mode, starts from about 64 Hz. Although not illustrated in Fig. 2, it was found that the lowest two nodal circle mode (2,0) starts from about 190 Hz and the lowest three nodal circle mode (3,0) from about 370 Hz. The frequencies of the backward traveling $(0,2)_b$ and $(0,3)_b$ modes become zero just above 600 rpm. This rotational speed corresponds to the critical speeds of the associated modes. The $(0,4)_b$, $(0,5)_b$, and $(0,6)_b$ modes undergo critical speeds at about 730, 860, and 1000 rpm, respectively. No apparent instability can be observed above the critical speeds in this case.

As seen in this figure, the deviation of the natural frequencies from those of the free disk is negligible in the low and middle frequency ranges. However, a remarkable change of frequency is noted in the high-frequency range. From additional calculations to investigate the effects of I_ϕ and k_ϕ separately, it was found that a k_ϕ of this amount does not change the frequency from that of the free disk. Therefore, the change of the natural frequency from that of the free disk in the high-frequency range is caused by the I_ϕ only. As seen in Fig. 2, the change of frequency from the free disk can be noted from around 100 Hz, which is above the original natural frequency of the pitch vibration system f_ϕ. The effect of I_ϕ on the frequency becomes stronger for higher nodal-diameter modes. From a detailed examination of the frequency change above 100 Hz, it was found that the frequency change due to I_ϕ occurs in such a way that the top corner and the two upper-side frequency lines of each diamond or upper triangle shift downward, keeping the two side corners at the initial crossing points for the free disk. As seen from the high-frequency range in Fig. 2, all frequency lines always pass through the original crossing points of different mode lines, as pointed out by Schajer (1984).

If the pitch stiffness k_ϕ increases by 100 times from the case of Fig. 2, instability regions appear above the critical speeds as shown in Fig. 3. In this figure, the same symbols in the frequency f and the real part α represent the corresponding imaginary and real parts of a pair of complex conjugate eigenvalues. Except for the case of zero frequency, each single symbol in f corresponds to a conjugate pair of pure imaginary eigenvalues, since the corresponding α value is zero. At the rotational speed ω where f decreases to zero, the eigenvalues become a pair of positive and negative reals with the same absolute value. This implies that one of the modes with zero frequency becomes unstable. Since the zero-frequency mode is a stationary mode, this type of instability is termed here as a "stationary-type instability." The overlapped symbols in f also correspond to positive and negative reals with the same absolute value in α. This means that two modes have the same frequency, and that one of them is unstable. At this point the frequency curves of the two different modes are merged into one. Thus, this type of instability is termed here as a "merged-type instability."

Each stationary-type instability appears to start from near the critical speed described above. The rule that determines the onset of a merged-type instability is more complex. The merged-type instability apparently takes place when a reflected increasing frequency line and a decreasing frequency line meet in the neighborhood of a third line. As seen in the range 800–1000 rpm in Fig. 3, more than one instability of different types, or the same type, can occur at the same rotational speed.

From the calculated results for the case where only large pitch moment of inertia of $I_\phi = 10^2 \times I_{\phi 0}$ is included, it was found that the merged-type instabilities are also induced. However, its illustration and detail discussion are omitted here, because the characteristics of this instability are qualitatively similar to those due to the transverse mass which will be discussed later.

Small frequency changes from those for the free disk, such as a veering feature (Schajer, 1984), can be noted at crossing points between different mode lines in Fig. 3. Therefore, it is

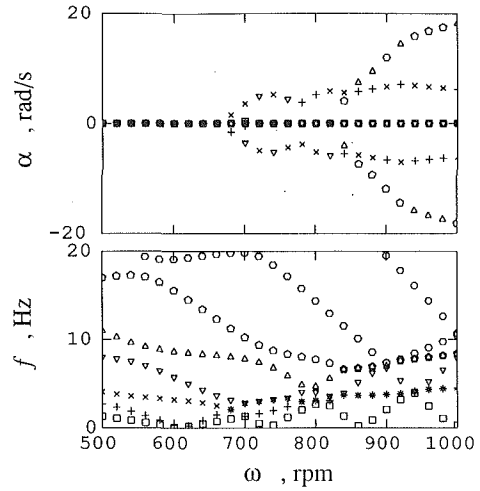

Fig. 6 Instability due to transverse mass only ($m_z = m_{z0}$)

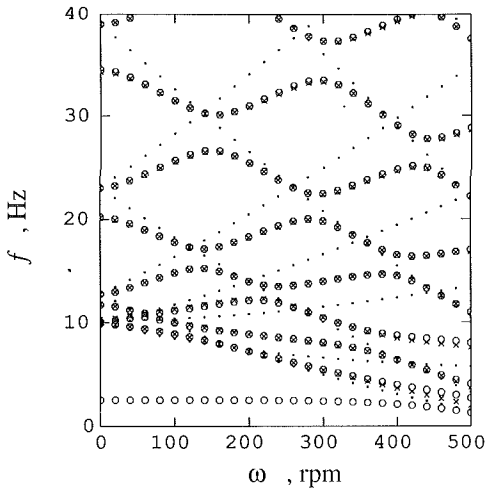

Fig. 7 The frequency change due to transverse mass and large transverse stiffness (o: transverse mass only [$m_z = m_{z0}$]; ×: transverse stiffness only [$k_z = 10^4 \times k_{z0}$]; •: freely spinning disk)

also interesting to examine the effect of increased pitch stiffness on natural frequency. For this purpose, the low and high-frequency ranges in the rotational speed range less than 500 rpm are depicted in Fig. 4 for the same parameters as in Fig. 3. From the comparison between Figs. 4 and 2, it is noted that the large deviation of f in the high-frequency range caused by moment of inertia is thoroughly suppressed by the increased pitch stiffness. Since the stiffness effect becomes predominant over the mass effect in the low-frequency range, all frequencies increase from the free disk values except for the (0,0) mode and the original crossing points of different modes. Compared with the frequency change due to moment of inertia, the frequency change due to stiffness takes place in the opposite direction such that the bottom corner and the lower two-side frequency lines of each diamond or the bottom-side frequency line of each upper triangle move upward, keeping the two side corners fixed at the initial crossing points for the free disk.

Moreover, it is interesting and worth noting that all frequencies above about 320 Hz decrease from the free disk values. Considering that the pitch vibration system attached to the disk has the natural frequency of 316 Hz in this case, we found that a general rule of frequency change due to the combination of pitch moment of inertia and pitch stiffness can be explained as follows: The inertia effect to decrease frequency and the stiffness effect to increase frequency are competitive with each other and the two effects are canceled just at the natural frequency f_ϕ of the pitch vibration system attached to the disk. The frequency of the disk below f_ϕ increases due to the dominance of the stiffness effect, while the frequency of the disk above f_ϕ decreases due to the dominance of the inertia effect. The degree of frequency deviation from the free disk values in the regions below and above f_ϕ increases with an increase in the pitch stiffness and inertia. Since the original $(n,0)$ mode motions have no pitch component, their frequencies are never affected by the pitch parameters, as seen in Fig. 4.

Although not illustrated, it was found from the additional parameter studies where large amounts of I_ϕ and k_ϕ are taken into account separately, that the frequencies asymptotically approach certain limiting values with an increase in pitch inertia, and these limiting frequency values are the same as are obtained with an increase in pitch stiffness, except the lowest natural frequency. The lowest natural frequency tend to zero with an increase in pitch inertia. These behaviors will be discussed in more detail in the case of transverse mass and stiffness effects.

(2) Transverse Mass and Stiffness Effects. Next, the transverse mass and stiffness effects on the eigenvalues are investigated. Figure 5 shows the destabilized eigenvalues due to a transverse mass of m_{z0} and a large transverse stiffness of $10^4 \times k_{z0}$. These values are regarded as close to the effective mass and stiffness of an actual head assembly in normal operating conditions. The natural frequency of the transverse mass and stiffness system f_z is 1.0 kHz in this case.

It is seen from Fig. 5 that this combination of m_z and k_z is large enough to cause instability after the critical speed. From additional calculated data for the cases where only m_z or k_z is taken into account separately, it was found that the eigenvalues in the presence of k_z only are the same as in Fig. 5 in all frequency ranges less than 400 Hz, and therefore the stiffness effect is predominant in these ranges. The eigenvalues in the presence of m_z only are found to be different from Fig. 5 in the low-frequency range, and are depicted in Fig. 6 for comparison.

As seen in Fig. 5, both stationary and merged-type instabilities again appear due to the transverse stiffness. By comparison of Fig. 5 with Fig. 3, one can note that the instability regions due to transverse stiffness only or dominant stiffness are fairly similar to those due to pitch stiffness. On the other hand, transverse mass gives rise to only the merged-type instability, as seen in Fig. 6. The reason why transverse mass and pitch inertia do not induce the stationary-type instability is that the inertia effects always vanish at zero frequency. If a large number of modes are taken into account, the unstable speed region caused by the transverse mass appears to be bounded differently from the Iwan and Moeller (1976) results where a few modes were taken into account.

It is worth noting that the frequencies f in Figs. 5 and 6 have the same values except in the low-frequency region where the merged-type instabilities take place. This suggests that f approaches a limiting value with an increase in stiffness only, and that this limiting value is the same as the one which f approaches with an increase in mass only, except in the low-frequency region associated with instability.

For a more detailed examination of the changes in frequency due to transverse mass and stiffness, the natural frequencies for the two cases which include transverse mass of $10 \times m_{z0}$ or transverse stiffness of $10^4 \times k_{z0}$ separately are plotted in Fig. 7 with circle and cross symbols, respectively, in the low-frequency and low rotational speed ranges. For comparison the natural frequencies of the free disk are also shown with small dots. It is found from this figure that the natural frequencies are almost equal in both cases except for the lowest frequency line of the case with transverse mass only.

Regarding the mass effect on frequency, it was found from this figure and additionally calculated data that the lowest

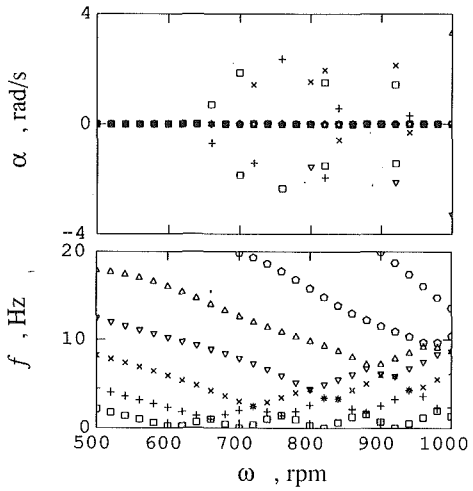

Fig. 8 Combination effect of I_ϕ, k_ϕ, m_z and k_z ($I_\phi = I_{\phi 0}$, $k_\phi = 10^3 \times k_{\phi 0}$ [f_ϕ = 316 Hz], $m_z = m_{z0}$, $k_z = 10^4 \times k_{z0}$ [f_z = 1.0 kHz]

frequency curve is reduced toward zero frequency as the transverse mass increases. At the same time the other frequencies decrease and approach asymptotic values in such a way that the top corner and two-side frequency lines of each diamond or triangle go down, keeping the two side corners at their original crossing points, similarly to the high-frequency region in Fig. 2. In the case where $m_z = m_{z0}$, the f value has not approached the asymptotic value, because the lowest frequency has not become zero and the f values with circles are slightly larger than the ones with cross symbols, as seen from Fig. 7. When the spinning disk is constrained by only transverse stiffness, on the other hand, the bottom corner and two-side frequency lines of each diamond or the bottom side of each triangle rise up from the free disk lines, keeping the two side corners at the same positions. As the transverse stiffness increases, the natural frequencies approach asymptotic values. In the case of Fig. 7, the transverse stiffness is so large that the natural frequency indicated by cross symbols is almost in the asymptotic state. It is seen from Fig. 7 that these limiting frequencies are equal except for the lowest frequency. However, it should be noticed that when both the mass and stiffness are combined together, the frequency changes can cancel each other near the natural frequency f_z of the attached mass and spring system, because the same asymptotic state is obtained by the decrease or increase of f depending on the mass or stiffness effect. From these results it can be said that the combination effects of the transverse mass and stiffness on the eigenvalues is also competitive rather than additive similarly to the combination effect of the pitch inertia and stiffness.

As mentioned before, the same behaviors as are described above for the transverse parameters can be obtained for the pitch parameters, although the limiting frequency values are different and the $(n,0)$ modes are not affected by pitch parameters.

(3) Combination Effect of Pitch and Transverse Parameters. An actual spinning disk in a floppy disk drive system is coupled with not only pitch moment of inertia and stiffness but also transverse mass and stiffness. So the next interest is to investigate the combined effects of the pitch and transverse parameters. Figure 8 shows the eigenvalues related to instability above the critical speed when the pitch parameters in Fig. 3 and the transverse parameters in Fig. 5 are taken into account at the same time.

It is worth noting that the unstable speed regions and the strength of the instability are markedly reduced by one fifth, as compared with Figs. 3 and 5. From the calculated data for the cases where only transverse and pitch stiffnesses are included, it was found that the instability characteristics are the same as shown in Fig. 8. This seems to imply that large pitch stiffness and large transverse stiffness can mutually suppress the strong instability tendencies indicated in Figs. 3 and 5. From the calculated results for the several cases where k_ϕ or k_z are further increased from the case in Fig. 8, it was found that the α values associated with instability change slightly but that the instability regions can neither be completely eliminated nor can they be increased again as in Fig. 3 or Fig. 5 by increasing k_ϕ or k_z. This implies that the combination effect of pitch and transverse stiffness on instability is neither additive nor competitive, but may be called a suppression effect.

From the additional parameter study where only I_ϕ and m_z are included, it was found that the instability characteristics above the critical speeds are governed by either I_ϕ or m_z, depending on their relative amounts. In other words, the combination effect of the pitch inertia and transverse mass is

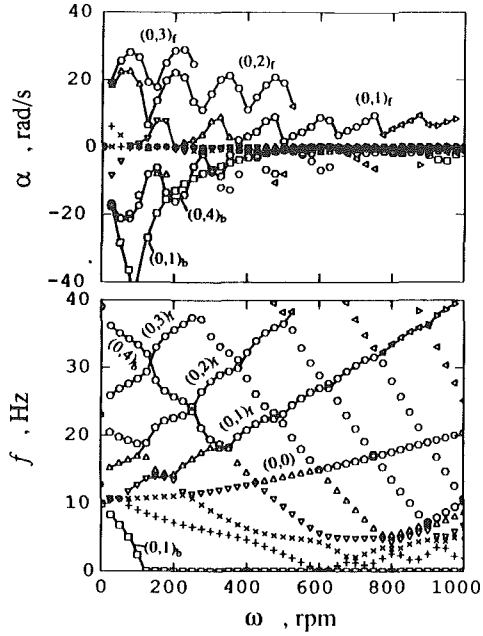

(a) Low frequency range

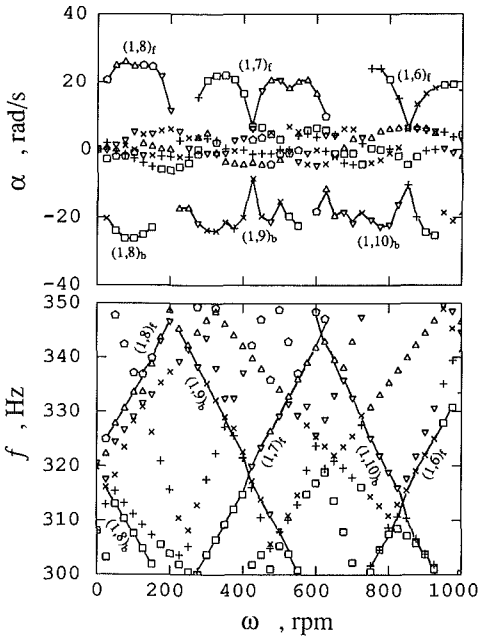

(b) High frequency range

Fig. 9 Friction effects on eigenvalues

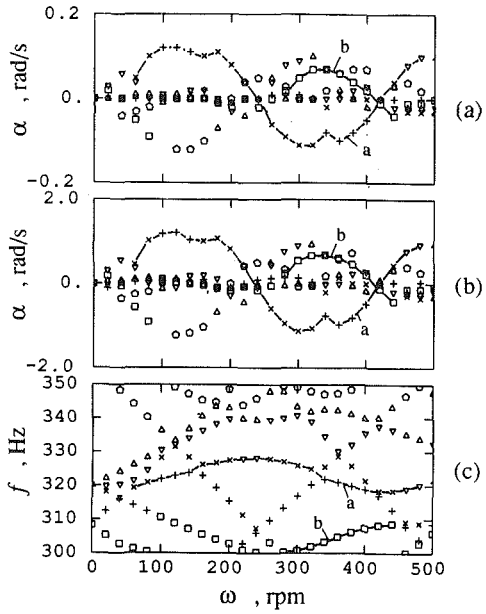

Fig. 10 Combination effect of friction force and other parameters on eigenvalues ($l_\phi = l_{\phi 0}$, $k_\phi = 10^3 \times k_{\phi 0}$, $k_z = k_{z0}$, $F_\theta = 0.32$ N); (*a*) real part values when $m_z = m_{z0}$; (*b*) real part values when $m_z = 0.1 \times m_{z0}$; (*c*) frequency when $m_z = m_{z0}$ or $0.1 \times m_{z0}$

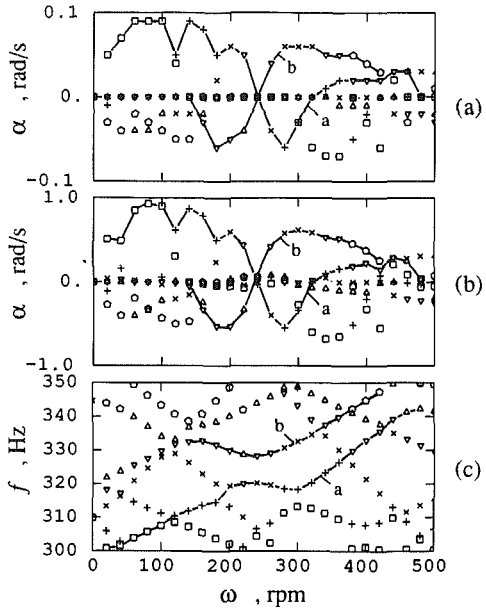

Fig. 11 Combination effect of friction force and other parameters on eigenvalues ($l_\phi = l_{\phi 0}$, $k_\phi = 10^2 \times k_{\phi 0}$, $k_z = k_{z0}$, $F_\theta = 0.32$ N); (*a*) real part values when $m_z = m_{z0}$; (*b*) real part values when $m_z = 0.1 \times m_{z0}$; (*c*) frequency when $m_z = m_{z0}$ or $0.1 \times m_{z0}$

competitive and any suppression effect as shown in Fig. 8 cannot be obtained. Therefore, a combination of two of the four parameters I_ϕ, k_ϕ, m_z and k_z usually affects the instability competitively except for the combination of k_ϕ and k_z.

The suppression effect due to the combination of k_ϕ and k_z may be hypothetically interpreted as follows: Modes destabilized by large pitch stiffness are possibly allowed to move only in the transverse direction, like a symmetrical deflection mode with respect to the coupling point. On the other hand, modes destabilized by large transverse stiffness are allowed to rotate about the coupling point, like a skew symmetrical deflection mode. Therefore, the former unstable modes may be suppressed by the addition of a transverse stiffness constraint, while the latter modes may be suppressed by a pitch stiffness constraint.

Since the values of pitch and transverse parameters considered in Fig. 8 are regarded as equivalent to those of an actual flexible disk drive in the normal operating condition, it can be said that the instability tendency above critical speeds can be largely removed by the constraints of pitch and transverse stiffnesses. However, the residual instability tendency cannot be eliminated without employing some other stabilizing means, such as a damping, as will be discussed later.

(4) Friction Effect. Next we investigate the instability effect of the head-disk friction force. In the following calculation, the static head load F_{z0} is assumed to be 0.4 N. The friction coefficient is considered as relatively large and is taken as 0.4. Then the tangential friction force F_θ is 0.32 N. Figures 9(*a*) and (*b*) show the eigenvalues in the low and high-frequency ranges, respectively, for the case where only the friction force is applied to the coupling point.

From the comparison of f values in Figs. 9(*a*) and (*b*) with those of the free disk in Fig. 2, it is found that the friction has an effect to change the frequencies from those of the free disk except for the $(n,0)$ modes. The reason for no change in the $(n,0)$ mode frequencies is that they have zero derivative in the circumferential direction so the static friction force effect vanishes as seen from the friction term in equation (1). The change of the frequencies from the free disk values and the veering feature near the crossing points are relatively stronger in the low-frequency range than in the high-frequency range. In particular, the $(0,1)_b$ mode frequency drops markedly and remains at zero above about 100 rpm.

As seen from the α values of Figs. 9(*a*) and (*b*), the instabilities are induced by constant friction force in the entire frequency range. Since the interaction between different original modes due to friction is not so strong, the notation of the corresponding original mode number is indicated for the typical increasing and decreasing frequency components for convenience. From comparison between the α and f values in Fig. 9, it is found that the forward, or increasing frequency, modes generally become unstable, while the backward, or decreasing, frequency modes remain stable. Near the crossing or veering points, the α values generally tend to zero. The steepness of the increasing or decreasing lines does not always result in a large absolute value of α. The largest positive α value appears in the $(0,3)_f$ mode in the low-frequency range, although the eigenvalues for higher-order modes are not illustrated in Fig. 9(*a*). In the high-frequency range between 300 and 350 Hz, on the other hand, the $(1,6)_f$, $(1,7)_f$, and $(1,8)_f$ mode lines have relatively large positive α values, while the $(1,8)_b$, $(1,9)_b$ and $(1,10)_b$ mode lines have relatively large negative α values. It is interesting to note in Fig. 9(*a*) that all the backward modes have small negative α values for frequency below the $(0,1)_f$ mode line, even above their critical speeds. The $(0,1)_b$ mode has a particularly large negative α value. From the rotational speeds above which the f values for the $(0,1)_b$ mode becomes zero, this conjugate eigenvalue changes to two negative values.

In an actual floppy disk drive, the static friction force is imposed on the disk together with pitch and transverse parameters. Therefore, we next calculated the combination effect of the friction force and the large pitch and transverse parameters which were used for the case in Fig. 8. The calculated result was found to be the same as in Fig. 8 in the entire speed range up to 1000 rpm and in the frequency range up to 400 Hz. The absolute value of α for any mode is reduced to less than 0.02 rad/s except the ones which are related to stationary (zero frequency) and merged-type instabilities. This means that the destabilizing effect of friction force is completely suppressed by the combination effects of large pitch and transverse stiffnesses.

Although the present analytical model may be still much simpler than the actual experimental set up used by Khono

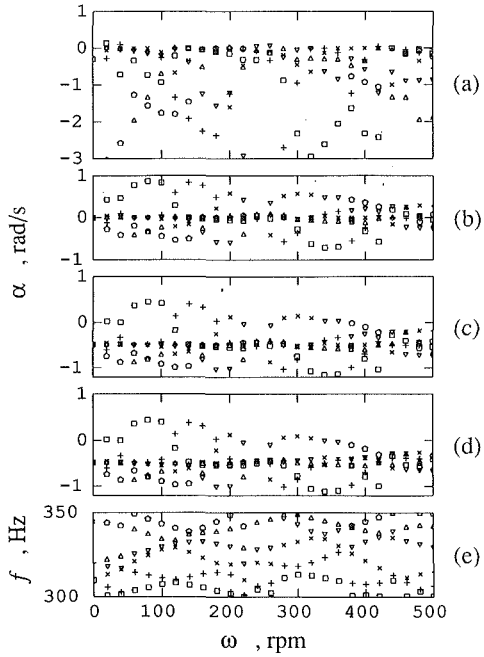

Fig. 12 Effect of damping factors c_ϕ, c_z, c_1, and c_2 on eigenvalues ($I_\phi = I_{\phi 0}$, $k_\phi = 10^2 \times k_{\phi 0}$, $k_z = k_{z0}$, $F_\theta = 0.32$ N); (*a*) $c_\phi = 2.01 \times 10^{-7}$ Nms/rad ($= 0.2\sqrt{I_\phi k_\phi}$); (*b*) $c_z = 1.59 \times 10^{-2}$ Ns/m ($= 0.2\sqrt{m_z k_z}$); (*c*) $c_1 = 0.1$ Ns/m; (*d*) $c_2 = 0.1$ Ns/m; (*e*) frequency for the cases (*a*), (*b*), (*c*), and (*d*)

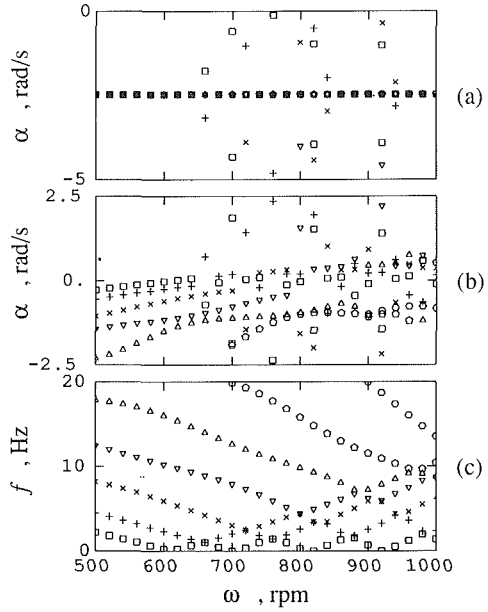

Fig. 13 Effect of damping factors c_1 and c_2 on instability above critical speeds ($I_\phi = I_{\phi 0}$, $k_\phi = 10^3 \times k_{\phi 0}$ [$f_\phi = 316$ Hz], $m_z = m_{z0}$, $k_z = 10^4 \times k_{z0}$ [$f_z = 1.0$ kHz]); (*a*) real part values for $c_1 = 0.5$ Ns/m; (*b*) real part values for $c_2 = 0.5$ Ns/m; (*c*) frequency for $c_2 = 0.5$ Ns/m

and et al. (1989), it is interesting to compare their observed characteristics of unstable vibration in the flexible disk and head assembly system with the calculated results obtained from the present model. According to their observation, typical features of unstable vibration are that the instability occurs in a certain rotational speed range and its frequency increases with increase in rotational speed. These features agree well with the characteristics of unstable vibration caused by friction force only, as shown in Figs. 9(*a*) and (*b*). In the normal operating condition, however, the transverse stiffness is so high, because of the fixed lower head, that the instability due to friction force can be thoroughly suppressed, as stated above. Therefore, if we imagine that the leading and trailing disk supporters used in their experiment have no function to stabilize a particular mode, and that the lift of the leading disk supporter functions to weaken the suppressing effect of mass and stiffness, then one of the interesting modes can possibly become unstable in a certain rotational speed region whose terminations correspond to veering points; for example, the $(1,7)_f$ mode becomes unstable between 425 and 600 rpm and the frequency may change from 320 to 347 Hz with increase in the rotational speed, as seen from Fig. 9(*b*). According to their description, the unstable vibration may have nodes near the disk supporters and may be regarded as a higher-order mode like the $(1,7)_f$ mode. Accordingly, it is reasonable to consider that the lift of the leading-side disk supporter induces some reduction in the transverse stiffness. For example, strong air-bearing effects may be developed between the lower head slider and the disk. If the loading arm and slider are decoupled, the effective mass of m_{z0} ($= 10m_s$) may be reduced to the slider mass m_s.

In order to investigate the possibility of friction instability under such abnormal conditions with reduced values of stiffness and mass parameters as described above, the eigenvalue analysis was further carried out for the four cases which include friction force as in Fig. 9 and the decreased pitch and transverse parameter values. If the transverse stiffness decreases to k_{z0}, the α values increase to more than 10 rad/s in the low-frequency range, but still remain less than 0.2 rad/s in the high-frequency range. In order to increase the α values in the high-frequency range, it is also necessary to decrease the transverse mass. The parameter study was done for the following four cases: (1) $k_z = k_{z0}$ with the other parameters having the same values as in Fig. 8, (2) $k_z = k_{z0}$, $m_z = 0.1 \times m_{z0}$ and the other parameters the same as in Fig. 8, (3) $k_z = k_{z0}$, $k_\phi = 10^2 \times k_{\phi 0}$ and the other parameters the same as in Fig. 8, and (4) $k_z = k_{z0}$, $m_z = 0.1 \times m_{z0}$, $k_\phi = 10^2 \times k_{\phi 0}$ and the other parameters the same as in Fig. 8.

If we confine our discussions only to the characteristics of eigenvalues in the high-frequency range, it was found that cases (1) and (2) have the same f values but different α values, and that cases (3) and (4) have the same f values but different α values. Thus, the α values for the cases (1) and (2) and their identical frequency f in the high-frequency range are shown in Figs. 10(*a*), (*b*), and (*c*), respectively. Similarly, Figs. 11(*a*), (*b*), and (*c*) show the corresponding quantities for the cases (3) and (4).

It is seen from these figures that the α values decrease almost inversely proportional to the increase in m_z in both Figs. 10 and 11 and that the f values in the high-frequency range depend not on m_z but on k_ϕ in these ranges of parameter values. The reason why m_z does not apparently change the f values, while changing the α values, is considered to be as follows: Since f_z is 31.6 Hz at most in these cases, the m_z effect is predominant over the k_z effect in the high-frequency range and the eigenvalues in Figs. 10 and 11 are close to the limiting state, in terms of the transverse mass effect, where the α values are zero.

For better understanding, the α and f lines of typical eigenvalues with relatively large α values are indicated with the same letters. Along the lines denoted by (*a*) and (*b*) in both Figs. 10 and 11, the same relationship between the slope of f and the sign of α as observed in Fig. 8 still holds. However, the increasing frequency regions with relatively large α values of the lines (*a*) and (*b*) in Fig. 10(*c*) are remarkably reduced compared with those in Fig. 11(*c*). As seen in Fig. 11, the mode indicated with (*a*) becomes unstable in the rotational speed region from 325 to 473 rpm. In this unstable region the unstable vibration frequency increases from 320 to 340 Hz, with an increase in the rotational speed. Similarly, the mode denoted by (*b*) becomes unstable in the rotational speed region from 240 to 440 rpm and the frequency increases from 330 to 350 Hz. It can be said that these results are in good qualitative

agreement with the experimental ones observed by Kohno et al. (1989).

From these parameter studies it is obvious that the instability caused by friction force can be suppressed by increasing the transverse stiffness and mass. From additional parameter studies it was also found that the friction instability can be suppressed by increasing the pitch moment of inertia and stiffness. The reason why the α values with $k_\phi = 10^3 \times k_{\phi 0}$ in Fig. 10 are larger than those with $k_\phi = 10^2 \times k_{\phi 0}$ in Fig. 11 is that the effect of I_ϕ and k_ϕ on the eigenvalues is almost canceled near 316 Hz, because $f_\phi = 316$ Hz in Fig. 10.

(5) Damping Effects. Lastly, we discuss the damping effects on the instability. To examine the effects of damping factors on the high-frequency instability caused by the friction force, we chose the abnormal case in Fig. 11(b) and (c), where $I_\phi = I_{\phi 0}$, $k_\phi = 10^2 \times k_{\phi 0}$ ($f_\phi = 100$ Hz), $m_z = 0.1 \times m_{m0}$ ($= m_s$), $k_z = k_{z0}$ ($f_z = 31.6$ Hz) and $F_\theta = 0.32$ N. The values of the damping coefficients c_ϕ and c_z are chosen to be 2.01×10^{-7} Nms/rad and 1.59×10^{-2} Ns/m, which correspond to 0.1 nondimensional damping ratios. Although the c_1 and c_2 values are not known, they both are chosen to be 0.1 Ns/m.

Figure 12 shows the α values for each case where only one damping factor described above is additionally taken into account. Since damping factors of this amount have no visible effect on frequency, the f values shown in Fig. 12(e) are common for the four cases. Similarly to the previous figures, the same symbols for α and f belong to a conjugate pair of eigenvalues. From Fig. 12(a) and (b) it is noted that c_ϕ has a strong stabilizing effect on the instability caused by friction force, whereas c_z has little stabilizing effect. However, this superiority of c_ϕ to c_z does not hold in the low-frequency range (not shown) where c_z has a rather stronger stabilizing effect than c_ϕ. It should be also noted from Fig. 12(a) that the α which originally had larger absolute values without c_ϕ move downward by a greater amount due to the addition of c_ϕ.

On the other hand, the damping factors c_1 and c_2 have different stabilizing effects such that all α values are shifted in the negative direction by the same amount, as seen from Figs. 12(c) and (d). Strictly speaking, some slight deviation from the uniform shift rule can be noted in Fig. 12(d) in the higher rotational speed region. It is obvious that this difference in the deviation of the α value with c_1 from that with c_2 results from the lack of the convective term of c_2 in equation (1).

From the additional parameter studies for the combination effects of these damping factors, it was found that they affect the α value under a simple principle of superposition, while keeping the f values unchanged, in the ranges of parameter values used here. It can be said from these results that the instability with high frequency caused by friction force can be effectively stabilized by the addition of a pitch damping to the suspension and some external damping to the disk.

Although not illustrated, it was found from the calculated results for the same parameters as in Fig. 11(b), but with damping, that the positive α values become more than 10 rad/s in the low-frequency range and these unstable vibrations of the lower-order modes cannot be stabilized by the four kinds of damping factors of this amount. In order to change the positive α value to negative, the amounts of c_ϕ, c_z, c_1, and c_2 should be increased by more than 20 times from those in Fig. 12. In an actual system, however, those lower-order modes would be practically suppressed by a disk liner, even if the transverse stiffness happens to be small.

In order to develop a high-speed flexible disk drive, on the other hand, it is well known that we should develop some means of increasing the external damping, for example, such as a Bernoulli plate. Therefore it is interesting to investigate the effect of strong surrounding air damping c_1 and c_2 on the instability in the high rotational speed region above the critical speeds. For the purpose of this parameter study, we chose three different combinations of the transverse and pitch parameters, as have already been treated in the above discussion. The first is the same as in Fig. 5 (large transverse mass and stiffness). The second is the same as in Fig. 8 (small pitch inertia and large pitch stiffness together with large transverse mass and stiffness). The third is the case having the same parameters as in Fig. 11(b) excluding the friction force (small pitch and transverse parameter values). Currently available high rotational speed flexible disk drives with a fixed recording head and some stabilizing plate may be modeled as the one with parameter values between the first and second cases. If a pair of flying head sliders are employed, similarly to those rigid disk drives, the head and suspension system is modeled as the third case. In high-speed flexible disk drive, the friction force should be decreased to be negligible value in any case. For each case described above, the external damping effects were examined by calculating three cases where $c_1 = 0.5$ Ns/m, $c_2 = 0.5$ Ns/m and $c_1 = c_2 = 0.5$ Ns/m are added separately.

Since it was found that the external damping effects on the eigenvalues are essentially equivalent for all three cases of different combinations of the pitch and transverse parameters, the c_1 and c_2 effects on the f and α values in the second case are representatively shown in Fig. 13. Figure 13(a) portrays the α values in the case where only c_1 is included. The corresponding f values are just the same as shown in Fig. 8. From the comparison between the α values in Fig. 8 and those in Fig. 13(a), it is seen that the α values for all modes uniformly shift to the negative direction and almost all unstable modes are stabilized except for the one which emerges at 1000 rpm (α value is off the graph). As seen from the comparison between Fig. 12(c) and Fig. 13(a), the amount of negative shift in the α values due to c_1 is proportional to the c_1 value. Therefore, it can be said that all unstable modes can be stabilized by the addition of the necessary amount of the spinning external damping factor c_1.

Figures 13(b) and (c), respectively, show the α and f values when only $c_2 = 0.5$ Ns/m is included. From careful comparison of the f values in Fig. 13(c) with those in Fig. 8, it is found that some of the merged frequencies in Fig. 8 separate by small amounts due to the c_2 effect in Fig. 13(c). Even though the two frequencies are not merged, the original pair of positive and negative α values remain unchanged excluding a few exceptions such as the pairs observed at 840 and 940 rpm. From Fig. 13(b) it is found that the α value of every backward mode increases from the same negative value as is obtained by the same amount of c_1 and becomes positive just above the corresponding critical speed, as the rotational speed increases. The eigenvalues of the stationary-type instability modes are not affected by the addition of c_2. As the rotational speed increases further, the increasing frequency lines which reflect back at the critical speeds cross the decreasing frequency lines of the other backward modes, and the α values of the two crossing modes become a large positive and negative pair near the crossing points, even if the two frequencies do not merge into one. By careful inspection to the correspondency between the α in Fig. 13(b) and the f in Fig. 13(c) near the crossing point, it is noted that the α value of the decreasing frequency line jumps to the negative value of the pair, while that of the increasing frequency line jumps to its positive value. On the whole, it is found that the stationary external damping factor c_2 has no effect to stabilize the instability above the critical speed caused by the pitch and transverse inertias and stiffnesses. On the contrary, all backward modes become unstable, although the amounts of the positive α values remain small.

From the calculated results for the case where both c_1 and c_2 are included, it was also found that the α values are equal to the sum of the two cases where c_1 and c_2 are separately

included and that the f values are nearly equal to the ones where only c_2 is included.

Conclusions

A new modeling and theoretical formulation is presented including friction force and pitch motion of a head slider as well as its transverse motion. The results of an eigenvalue analysis for a 5.25-in. flexible disk drive system with various values of the related parameters can be summarized as follows:

1 Large pitch moment of inertia and large pitch stiffness have destabilizing effects on the backward travelling modes above their critical speed similarly to transverse mass and stiffness.

2 Large pitch and transverse stiffness induce two kinds of instability above critical speeds; stationary (zero frequency)-type instability and merged-type instability. Every unstable speed region is bounded.

3 Large pitch moment of inertia and transverse mass causes only the merged-type instability above critical speeds. The unstable speed region is also bounded.

4 Pitch moment of inertia and transverse mass attached to the disk shift downward the original free-disk frequency lines, except for the crossing points of two different frequency lines. On the other hand, the pitch and transverse stiffness shift upward the original frequency lines, excluding the crossing points. In case of pitch parameters, the eigenvalues of the original zero-nodal diameter modes do not change.

5 With an increase in transverse mass, the frequency lines approach certain limiting lines which are the same as the frequency lines approach with increase in transverse stiffness, with the exception of the lowest frequency line. The lowest frequency line tends to zero with an increase in the transverse mass. The same situation occurs in the relation between the pitch moment of inertia and stiffness. The limiting frequency lines are different for the transverse and pitch parameters.

6 The combination effects of pitch inertia and stiffness or transverse mass and stiffness on eigenvalues are competitive. The two effects are canceled at the mass-stiffness natural frequencies, above which the inertia or mass effect becomes predominant and below which the stiffness effect becomes predominant.

7 The positive real part values of the unstable modes caused by the pitch stiffness and transverse stiffness separately can be largely reduced by the combination of the pitch and transverse stiffnesses. This suppression effect of instability cannot be observed in the combination of the pitch moment of inertia and transverse mass.

8 A constant friction force makes every increasing frequency mode unstable and every decreasing frequency mode stable over the entire rotational speed region, except the original zero-nodal diameter mode. Near the crossing points between the increasing and decreasing frequency lines, the real part values tend to be zero. This result shows good correlation with prior experimental ones.

9 The instability due to the friction force can be suppressed by increasing the transverse mass and stiffness and pitch stiffness. In the normal operating condition of an actual flexible disk drive with a lower fixed head, the friction instability is regarded as completely suppressed due to large transverse stiffness and large effective transverse mass. However, if the constraints due to the large transverse stiffness and mass are accidentally released, the instability due to the friction force may appear.

10 The unstable vibration with high frequency caused by the friction force can be effectively stabilized by the pitch damping of the head suspension. The transverse damping of the head suspension has little stabilizing effect on the high-frequency unstable modes. The external rotating and stationary dampings also have a stabilizing effect on the friction instability. The degrees of the stabilizing effects are proportional to the amount of each damping factor and the combination effect of different damping factors is additive.

11 The instability caused by pitch stiffness and transverse mass and stiffness above the critical speed can be stabilized by increasing the effect of spinning external damping. The stationary external damping has no stabilizing effect on the instability of this kind. In addition, the stationary external damping has a small destabilizing effect on all backward modes above the critical speeds.

References

Benson, R. C., and Bogy, D. B., 1978, "Deflection of a Very Flexible Spinning Disk due to a Stationary Transverse Load," ASME JOURNAL OF APPLIED MECHANICS, Vol. 45, pp. 636–642.

Good, J. K., and Lowery, R. L., 1985, "The Finite Element Modeling of the Free Vibration of a Read/Write Head Floppy Disk System," ASME *Journal of Vibration, Acoustics, Stress, and Reliability in Design*, Vol. 107, pp. 329–333.

Iwan, W. D., and Moeller, T. L., 1976, "The Stability of a Spinning Elastic Disk With a Transverse Load System," ASME JOURNAL OF APPLIED MECHANICS, Vol. 43, pp. 485–490.

Jiang, Z. W., and Chonan, S., 1989, "Optimum Design of a Read/Write Head Floppy Disk System," *Proc. Int. Conf. Advanced Mechatronics*, Tokyo, pp. 325–330.

Kohno, T., Matsushita, O., Terayama, T., and Nemoto, Y., 1989, "Unstable Vibration of Head Assembly in Flexible Disk Drive Unit," *Proc. Int. Conf. Advanced Mechatronics*, Tokyo, pp. 319–324.

Ono, K., Maeno, T., and Ebihara, T., 1986, "Study on Mechanical Interface Between Head and Media in Flexible Disk Drive (2nd Report, Dynamic Response Characteristics due to a Concentrated Force)," *Bulletin of the JSME*, Vol. 29, No. 255, pp. 3109–3115.

Ono, K., and Maeno, T., 1987, "Theoretical and Experimental Investigation on Dynamic Characteristics of a 3.5-Inch Flexible Disk due to a Point Contact Head," *Tribology and Mechanics of Magnetic Storage Systems*, Vol. 3, SP.21 (STLE), pp. 144–151.

Schajer, G. S., 1984, "The Vibration of a Rotating Circular String Subject to a Fixed Elastic Restraint," *Journal of Sound and Vibration*, Vol. 92, No. 1, pp. 11–19.